J Mar Sci Technol (2016) 21:38–47
DOI 10.1007/s00773-015-0330-5

ORIGINAL ARTICLE

A feature-matching method for side-scan sonar images based on nonlinear scale space

Xiu-Fen Ye[1] · Peng Li[1] · Jian-Guo Zhang[1] · Jian Shi[1] · Shu-Xiang Guo[1,2]

Received: 19 March 2015 / Accepted: 28 June 2015 / Published online: 16 July 2015

Abstract We report a novel feature-matching method for side-scan sonar images. The method uses nonlinear diffusion filtering to build a nonlinear scale space. The noise-reduction performance is enhanced via nonlinear diffusion filtering, and the improved Perona–Malik diffusion equation results in a more distinct edge and line texture in the side-scan sonar image. The modified feature descriptor reduces the dimensionality of the feature vector so that the computational expense is reduced. Experimental results show that the method provides improved noise-reduction performance and better accuracy than SIFT, SURF, and other state-of-the-art feature-matching algorithms.

Keywords Feature matching · Side-scan sonar image · Nonlinear scale spaces

1 Introduction

The use of side-scan sonar systems together with image-matching techniques has been particularly useful for ocean exploration and undersea object detection and recognition. However, feature matching is often very difficult in undersea applications because there is typically a large amount of reverberation noise as well as a low signal-to-noise ratio, and furthermore, features of sonar images of objects under the seafloor are very rarely compared with optical images [1, 2].

There have been a number of methods used for sonar image matching, including using the highlight area and shadow zone of sonar images [3]; however, this only works for images with no orientation or scale change. Rominger used the theory of belief functions to obtain the optimal transformation in the registration progress [4]; however, this incurs a significant computational expense. It is also possible to extract the corner features of side-scan sonar images and match them using mutual correlation coefficients [5].

The development of multi-scale image registration methods has made it possible to match images at different scales or resolutions with improved accuracy. Vanish used the scale-invariant feature transform (SIFT) algorithm with side-scan sonar image registration and found that it performed better than previous methods [6]. The SIFT algorithm, which was first developed by Lowe in [7], is perhaps the most important achievement in image matching. It uses linear scale spaces built using a Gaussian filter to extract keypoints from images to perform reliable matching. The features are invariant with scale and rotation, and this method has been used in many different computer vision applications. However, SIFT is very computationally expensive and hence time consuming. The PCA-SIFT algorithm [8] and the speed up robust feature (SURF) algorithm [9] were proposed to overcome this problem. The neighborhood of the feature point, which is represented by a feature vector, is low-dimensional in PCA-SIFT to make matching faster, and the SURF algorithm uses integral images and box filters to improve the registration speed [10]. There have also been reports of SIFT-like methods, including CSIFT, GLOH, and ASIFT [11–13]. However, none of these methods can meet the requirements of real-time applications.

✉ Xiu-Fen Ye
yexiufen@hrbeu.edu.cn

1 College of Automation, Harbin Engineering University, Harbin 150001, Heilongjiang, People's Republic of China

2 Faculty of Engineering, Kagawa University, Hayashichou, Kagawa 2217-20, Japan

In the past 2 years, new algorithms based on binary strings have been developed, which can be used to describe the keypoints faster, including the oriented fast and rotated BRIEF(ORB) and fast retina keypoint (FREAK) methods [14, 15]. These algorithms use a linear scale space built using a Gaussian low-pass filter, which has hindered their application in side-scan sonar images. The most important data in the sonar image are the edge and the line textures. Therefore, when Gaussian blurring is applied to sonar images to reduce the noise, some detailed information is also lost, leading to registration failure. In ECCV 2012, Alcantarilla et al. exploited KAZE features and used nonlinear filters in image registration. The algorithm improved the repeatability and distinctiveness in the image matching [16], bilateral filter combined with SIFT method was developed to match synthetic aperture radar image features, it was found to perform better than SIFT in those images which were corrupted by speckle noise [17]; however, the price to pay is high time consumption because of the complexity of the bilateral filter for constructing scale space.

In this paper, we describe a novel feature-matching algorithm based on nonlinear scale space. We use the nonlinear diffusion equation to eliminate the effects of noise and, at the same time, enhance the edge and line textures in side-scan sonar images. The feature vector is simplified to speed up the calculation. The sufficient image information preserved and the simplified feature vector lead to an accurate and fast matching performance.

The remainder of this paper is organized as follows. In Sect. 2, we introduce the nonlinear scale space based on the Perona–Malik (P-M) nonlinear diffusion model; Sect. 3 focuses on the feature detection and descriptor for each keypoint in the nonlinear scale space; a comparison of the efficiency of our method with the existing algorithms is given in Sect. 4, together with experimental results. Conclusions are drawn in Sect. 5.

2 Construction of nonlinear scale space based on P-M model

2.1 P-M nonlinear diffusion model

The idea of processing images in scale space was first developed in the 1980s based on the heat equation, i.e.,

$$\begin{cases} \dfrac{\partial u}{\partial t} = \Delta u(x,y,t), & (x,y,t) \in \mathbb{R}^m \\ u(x,y,0) = u(x,y), & (x,y) \in \mathbb{R}^m \end{cases} \tag{1}$$

where $\mathbb{R}^m$ is a bounded open domain and $u(x,y,0) = u(x,y)$ is the original image; the solution of Eq. 1 is

$$u(x,y,t) = G_t * u(x,y) \quad t > 0 \tag{2}$$

$$G_t(x,y) = \frac{1}{\sqrt{4\pi t}} \exp\left(-\frac{x^2+y^2}{4t}\right) t > 0 \tag{3}$$

At time t, the solution of the heat equation smoothes the original image using a Gaussian low-pass filter. However, Eq. 1 is isotropic and smoothes the image identically in all directions, which does not preserve the edges. To solve this problem, Perona and Malik developed the P-M diffusion equation [18], i.e.,

$$\begin{cases} \dfrac{\partial u}{\partial t} = \operatorname{div}(g(|\nabla u|)\nabla u), & (x,y,t) \in \mathbb{R}^m \\ u(x,y,0) = u(x,y), & (x,y) \in \mathbb{R}^m \end{cases} \tag{4}$$

where div is the divergence operator and $g(|\nabla u|) = 1/\left(1 + \left(\frac{|\nabla u|}{K}\right)^2\right) \in [0,1]$ is termed the diffusion function or edge-stropping function and is a function of the magnitude of the gradient, and the parameter K is termed the diffusion constant and is typically fixed by hand. The diffusion function is adaptive to the edges of the image in the continuous region; when the magnitude of the gradient of the image is far $<K$, $g(|\nabla u|) \approx 1$, the image is smoothed. However, at the edges, the magnitude of the gradient is much $> K$, $g(|\nabla u|) \approx 0$, and the diffusion process is not carried out; the image will not be smoothed, thus preserving the edge.

2.2 Improved P-M equation

The P-M equation does not have a unique stable solution, which is a serious problem for sonar image matching. Two very similar images will typically result in divergent solutions and therefore different edges will also typically result in. Catte [19] provided a regularized model, i.e.,

$$\frac{\partial u}{\partial t} = \operatorname{div}(g(|\nabla G_\sigma * u|)\nabla u), \quad (x,y,t) \in \mathbb{R}^m \tag{5}$$

where G_σ is a Gaussian function with a variance σ. Catte proved that the image diffusion was stable and that Eq. 5 converges to a unique and constant stationary solution. Moreover, the diffusion function is significant for edge preservation and image smoothing. We use the following function to describe the diffusion behavior:

$$g(|\nabla u|) = \frac{1}{1 + \left(\frac{|\nabla u|}{K}\right)^\mu} \tag{6}$$

Note that the diffusion function used by Perona and Malik is a special case of Eq. 6 when $\mu = 2$.

Figure 1 shows the relationship between the diffusion function with the form of Eq. 6 and ∇u, and Fig. 2 shows a comparison of the P-M filter and our method. We can see

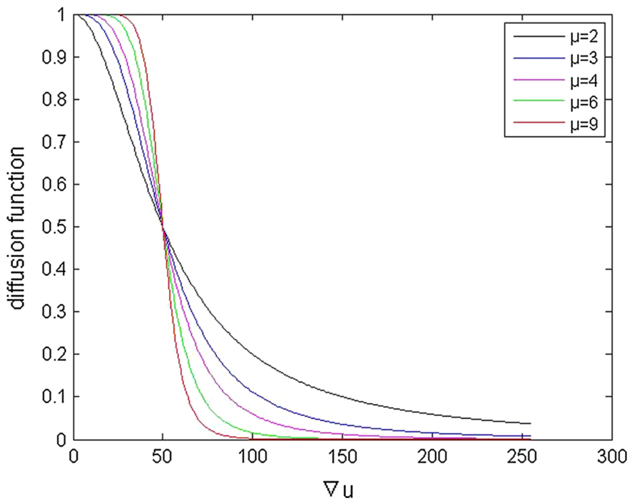

Fig. 1 The relationship between Eq. 6 and ∇u, $K = 50$

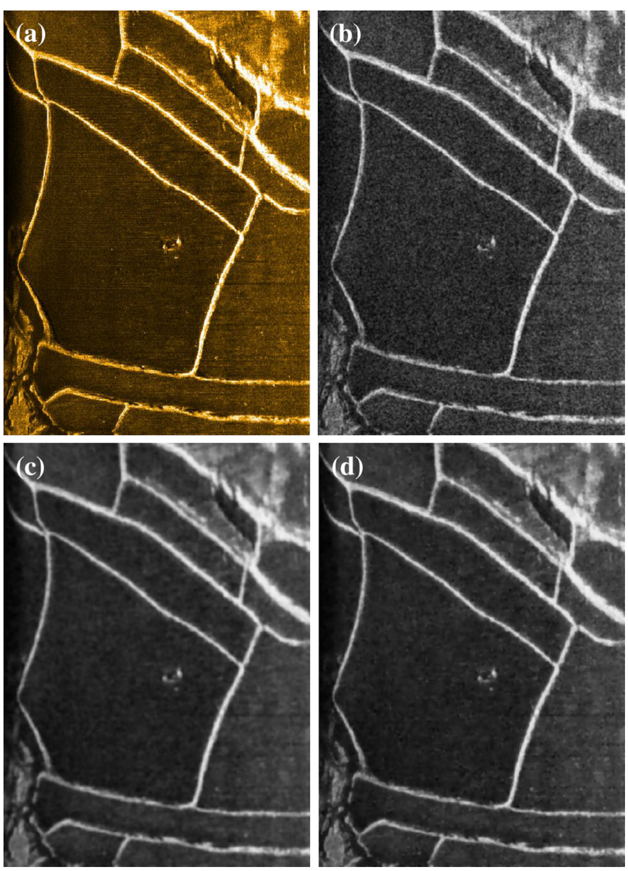

Fig. 2 The results of smoothed image after P-M filter. **a** Pseudo-color sonar image. **b** Image with serious noise. **c** P-M filter. **d** Improved P-M filter

that, as ∇u increases, a larger μ makes $g(|\nabla u|)$ tend to zero faster, and when ∇u decreases, a larger μ makes $g(|\nabla u|)$ tend to 1 faster. For convenient computation, we take $\mu = 4$ in this paper, and the revised P-M model can be written as

$$\begin{cases} \dfrac{\partial u}{\partial t} = \operatorname{div}(g(|\nabla G_\sigma * u|)\nabla u), & (x,y,t) \in \mathbb{R}^m \\ u(x,y,0) = u(x,y), & (x,y) \in \mathbb{R}^m \end{cases} \tag{7}$$

$$g(|\nabla G_\sigma * u|) = \frac{1}{1 + \left(\frac{|\nabla G_\sigma * u|}{K}\right)^4} \tag{8}$$

Let $T = \frac{1}{\sqrt{u_x^2+u_y^2}}\begin{pmatrix} u_x \\ u_y \end{pmatrix}$, $N = \frac{1}{\sqrt{u_x^2+u_y^2}}\begin{pmatrix} -u_y \\ u_x \end{pmatrix}$ are the unit vectors along the tangent and normal directions, $\cos\alpha = \frac{u_x}{\sqrt{u_x^2+u_y^2}}$, $\sin\beta = \frac{u_y}{\sqrt{u_x^2+u_y^2}}$ are direction cosines, then

$$\begin{aligned} u_T &= \frac{u_x^2+u_y^2}{\sqrt{u_x^2+u_y^2}}, \quad u_N = 0 \\ u_{TT} &= \frac{u_x^2 u_{xx} + 2u_x u_y u_{xy} + u_y^2 u_{yy}}{u_x^2+u_y^2} \\ u_{NN} &= \frac{u_x^2 u_{yy} - 2u_x u_y u_{xy} + u_y^2 u_{xx}}{u_x^2+u_y^2} \end{aligned} \tag{9}$$

$$u_{TT} + u_{NN} = u_{xx} + u_{yy}$$

Substituting Eqs. 8 and 9 into Eq. 7,

$$\begin{aligned} \frac{\partial u}{\partial t} &= div(g(|\nabla G_\sigma * u|)\nabla u) = div\left((g|\nabla G_\sigma * u|)\begin{pmatrix} u_x \\ u_y \end{pmatrix}\right) \\ &= \frac{\partial}{\partial x}(g(|\nabla G_\sigma * u|)u_x) + \frac{\partial}{\partial y}(g(|\nabla G_\sigma * u|)u_y) \\ &= \frac{\partial g(|\nabla u|)}{\partial|\nabla u|}\frac{\partial\left(\sqrt{u_x^2+u_y^2}\right)}{\partial x}u_x + \frac{\partial g(|\nabla u|)}{\partial|\nabla u|}\frac{\partial\left(\sqrt{u_x^2+u_y^2}\right)}{\partial y}u_y \\ &\quad + g(|\nabla u|)(u_{TT}+u_{NN}) \\ &= g(|\nabla G_\sigma * u|)u_T \\ &\quad + [g(|\nabla G_\sigma * u|) + g'(|\nabla G_\sigma * u|)|\nabla u|]u_N \\ &= G_\sigma * \frac{k^4}{k^4 + |\nabla u|^4}u_T + G_\sigma * \frac{k^4\left(k^4 - |\nabla u|^4\right)}{\left(k^4 + |\nabla u|^4\right)^2}u_N \end{aligned} \tag{10}$$

where $G_\sigma *$ is equivalent to the image smoothed with a Gaussian filter. In the continuous region, the magnitude of the gradient image is far $<K$; we then have

$$\begin{aligned} &\lim_{k\to\infty} g(|G_\sigma * \nabla u|) = G_\sigma * \lim_{k\to\infty}\frac{k^4}{k^4+|\nabla u|^4} = 1 \\ &\lim_{k\to\infty}[g(|G_\sigma * \nabla u|) + g'(|G_\sigma * \nabla u|)|\nabla u|] \\ &= G_\sigma * \lim_{k\to\infty}\frac{k^4\left(k^4 - |\nabla u|^4\right)}{\left(k^4+|\nabla u|^4\right)^2} = 1 \end{aligned} \tag{11}$$

Table 1 Evaluation of the image

μ	2	3	4	6	9
V_{Brenner}	609.66	646.23	847.92	505.34	506.49

The diffusion is applied and the image is smoothed; however, at the edge region, the gradient magnitude is far larger than K, and so we have

$$\lim_{|\nabla u|\to\infty} g(G_\sigma * \nabla u) = G_\sigma * \lim_{|\nabla u|\to\infty} \frac{k^4}{k^4 + |\nabla u|^4} = 0$$

$$\lim_{|\nabla u|\to\infty} [g(|G_\sigma * \nabla u|) + g'(|G_\sigma * \nabla u|)|\nabla u|]$$

$$= G_\sigma * \lim_{|\nabla u|\to\infty} \frac{k^4\left(k^4 - |\nabla u|^4\right)}{\left(k^2 + |\nabla u|^4\right)^2} = 0 \tag{12}$$

The diffusion is not applied, and so the edge is preserved.

Figure 2 shows the results of smoothed sonar image with P-M filter and the improved one. All the sonar images processed in this paper were obtained from a real side-scan sonar system from a lake.

We evaluate the definition of the smoothed image using the Brenner value [20], i.e.,

$$V_{\mathrm{Brenner}} = \sum_M \sum_N (f(x+2, y) - f(x, y))^2 \tag{13}$$

where $M \times N$ is the size of the image; the larger V_{Brenner} is, the higher the quality of the image. V_{Brenner} reaches highest when $\mu = 4$, as shown in Table 1, when μ is large than 4, the Brenner value goes down because the higher μ over-smoothes the images and destroy the detailed information. So our method preserves more edges and detail following smoothing than does the P-M filter.

2.3 Construction of the nonlinear scale space

To build the nonlinear scale space, images under all different scale levels are required; however, the nonlinear diffusion equation (Eq. 7) has no analytical solution. Weickert used a linear-implicit iterative method to solve this equation [21], and the discrete expression and its solutions are shown in Eqs. 14 and 15, respectively:

$$\frac{u^{i+1} - u^i}{\tau} = \sum_{d=1}^{m} A_d(u^i) u^{i+1} \tag{14}$$

$$u^{i+1} = \left(I - \tau \sum_{d=1}^{m} A_d(u^i)\right)^{-1} u^i \tag{15}$$

where A_d is the conductive d-dimensional matrix, it encodes the conductivities for the image. If $A_d(u^i)$ is constant, the diffusion will be linear. If $A_d(u^i)$ is a matrix of the same size as image u^i, the diffusion will be nonlinear. τ is the time step at any length, and I is the identity matrix.

As with SIFT, the discrete scale space is made up of a series of O octaves and S sub-levels, which correspond to a scale σ, i.e.,

$$\sigma_i(o, s) = \sigma_0 \cdot 2^{\frac{o+s}{S}}$$
$$o \in [0, \ldots, O-1], s \in [0, \ldots, S-1], i \in [0, \ldots, N] \tag{16}$$

where σ_0 is the initial scale level and N = O*S is the total number of images.

Because nonlinear filtering is diffuse with time, and we construct a nonlinear scale space using a set of evolution time points, the discrete scale levels in pixel units σ_{i} are mapped to time units t_i. The following mapping formula was used:

$$t_i = \frac{1}{2}\sigma_i^2, \quad i = \{0, \ldots, N\} \tag{17}$$

where t_i is the evolution time, which means that filtering an image at time t_i is equivalent to convolving an image with a Gaussian standard deviation σ.

Thus, given an input image, we can build the nonlinear scale space with evolution time through the diffusion equation, i.e.,

$$u^{i+1} = (I - (t_{i+1} - t_i) \cdot \sum_d^m A_d(u^i))^{-1} \cdot u^i \tag{18}$$

Figure 3 shows a comparison between the linear scale space built using the Gaussian filter and the nonlinear scale space for different evolution times using the P-M diffusion model. It is clear that, in the nonlinear scale space image, the edges are better preserved.

3 Feature extraction

3.1 Keypoints detection

As with the SIFT algorithm, we use the Hessian determinant to detect local extreme points, which are the points of interest at the multi-scale level. The Hessian matrix is defined as

$$H(f(x, y)) = \begin{bmatrix} \frac{\partial^2 f}{\partial x^2} & \frac{\partial^2 f}{\partial x \partial y} \\ \frac{\partial^2 f}{\partial x \partial y} & \frac{\partial^2 f}{\partial y^2} \end{bmatrix} \tag{19}$$

and the determinant of $H(f(x, y))$ is

$$\det(H) = \frac{\partial^2 f}{\partial x^2}\frac{\partial^2 f}{\partial y^2} - \left(\frac{\partial^2 f}{\partial x \partial y}\right)^2 \tag{20}$$

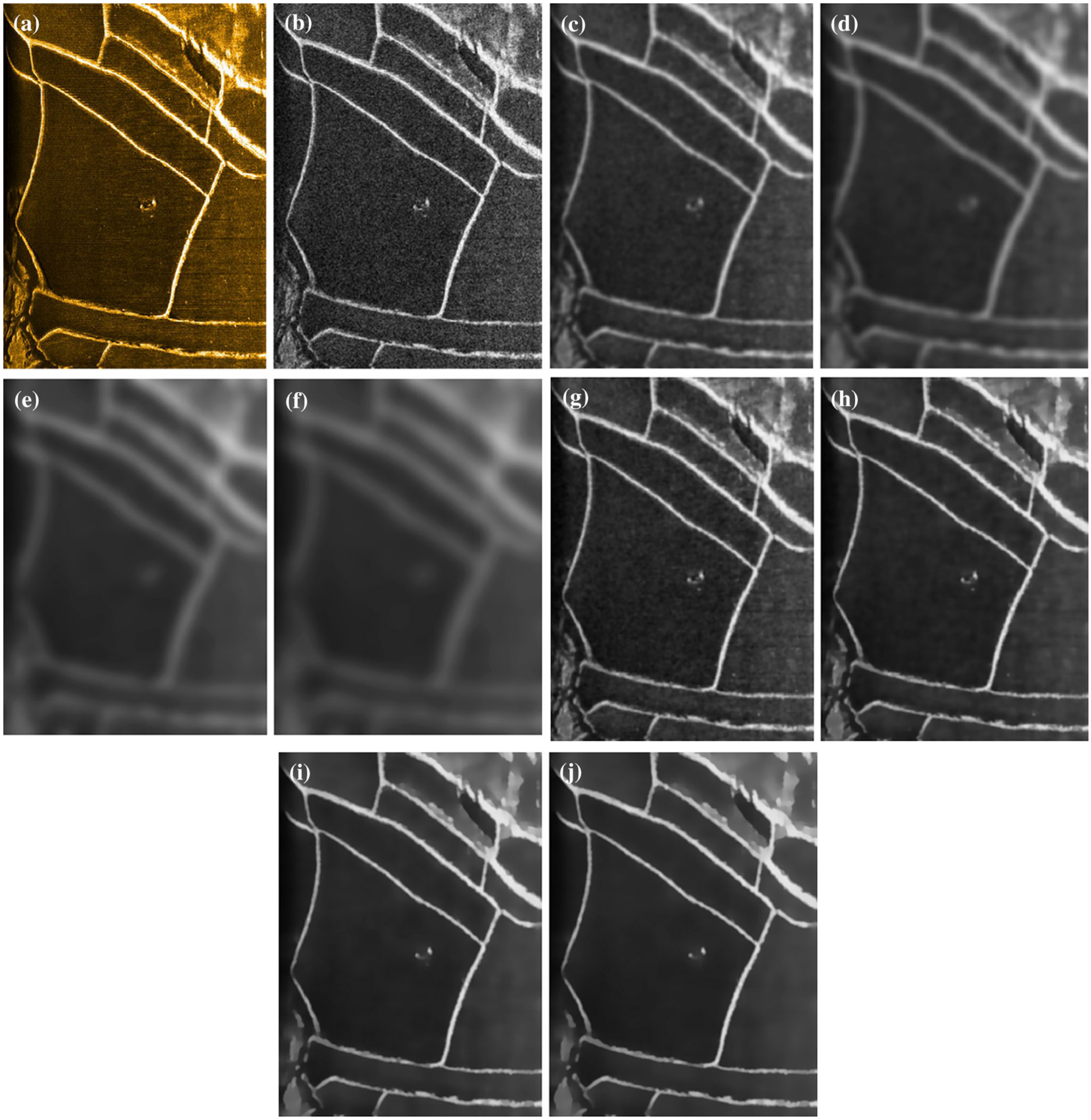

Fig. 3 The comparison between linear scale space built by Gaussian filter and nonlinear scale space for different evolution time through P-M diffusion model: **c**–**f** are linear scale space built by Gaussian filter with standard deviation of 3.2, 6.4, 12.8, 15.22; **g**–**j** are nonlinear scale space for evolution time of 5.12, 20.48, 81.92, 115.89 s

Replacing the value of the function $f(x, y)$ with the image pixel $u(x, y)$, we can obtain the Hessian matrix in the multi-scale image space, i.e.,

$$H(x, \sigma) = \begin{bmatrix} L_{xx}(x, \sigma) & L_{xy}(x, \sigma) \\ L_{xy}(x, \sigma) & L_{yy}(x, \sigma) \end{bmatrix} \tag{21}$$

The corresponding determinant is

$$\det(H(x, \sigma)) = \sigma^2 (L_{xx} L_{yy} - L_{xy}^2) \tag{22}$$

where L_{xx}, L_{yy}, and L_{xy} represent the second-order horizontal, vertical, and cross-derivatives, respectively. When looking for an extreme point, every pixel is compared with

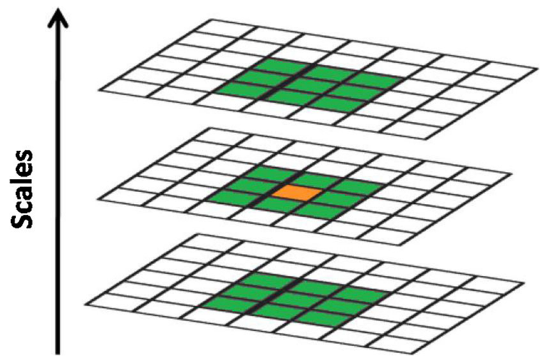

Fig. 4 The extreme detection at different scale spaces

its neighbor in the range of a cube of size 3 × 3 × 3. In Fig. 4, each sample pixel is compared with its nearest eight neighbors in the same scale image, and nine neighbors in the higher and lower scale images, which means that the pixel is compared with 26 neighbor pixels in 3 × 3 regions.

In SIFT algorithm, keypoints are obtained as the maxima and minima of the result of a Difference of Gaussians (DoG) operator applied through a Gaussian scale space. A pyramid of Gaussian blurred versions of the original image which are generated by down-sampling is computed to build the scale space, however, the proposed method always work with the original image resolution, without performing down-sampling as done in SIFT, make it more accurate to detect keypoints.

3.2 Feature vector description

To identify the main orientation for each keypoint, the first-order derivatives in the horizontal and vertical directions in a circle with a radius 6σ are calculated and weighted using a Gaussian function, σ, which is the scale level at the center of the keypoint. Rotating a fan-shaped window around the keypoint with a cover angle of 60° and summing the vector of derivatives, the longest vector corresponds to the main orientation of the keypoint, as shown in Fig. 5.

We selected a region aligned to the main orientation and centered at the keypoint, and then sampled the first-order derivatives in a 5 × 5 area every 60° in the horizontal and vertical directions. The derivatives are Gaussian weighted to form a four-dimensional vector $r = \left(\sum L_x, \sum L_y, \sum |L_x|, \sum |L_y|\right)$, where L_x and L_y represent the first-order derivatives. We took two circles of such samples, leading to a $6 \times 2 \times 4 = 48$ dimensional vector, as shown in Fig. 6, and normalized the vector to obtain the final descriptor.

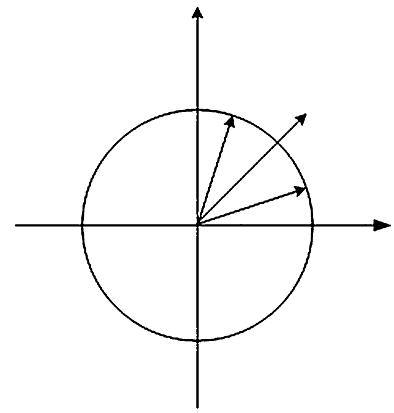

Fig. 5 A fan-shaped window slides around the keypoint to sum up the vector of derivatives responds

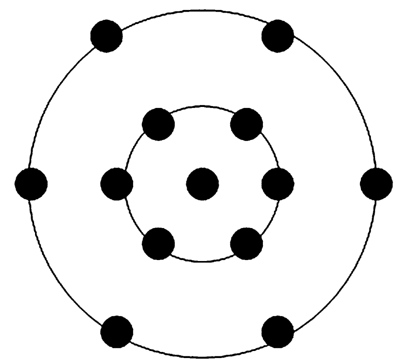

Fig. 6 Illustrated diagram of the descriptor

4 Experimental results

In this section, experimental results are discussed to assess the performance of the method. Data were obtained using Visual Studio 2008 with a 3.10-GHz core processor and

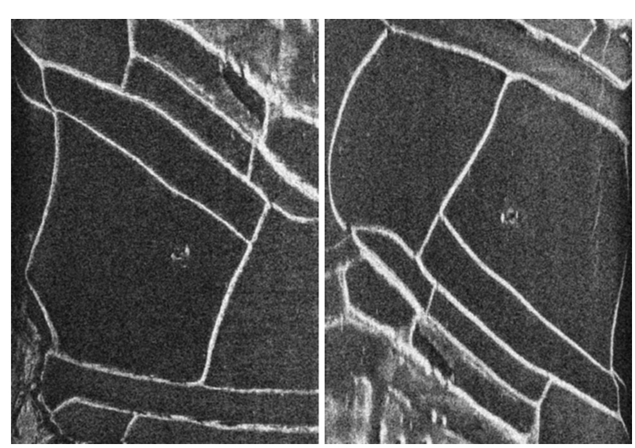

Fig. 7 Two side-scan sonar images with noise

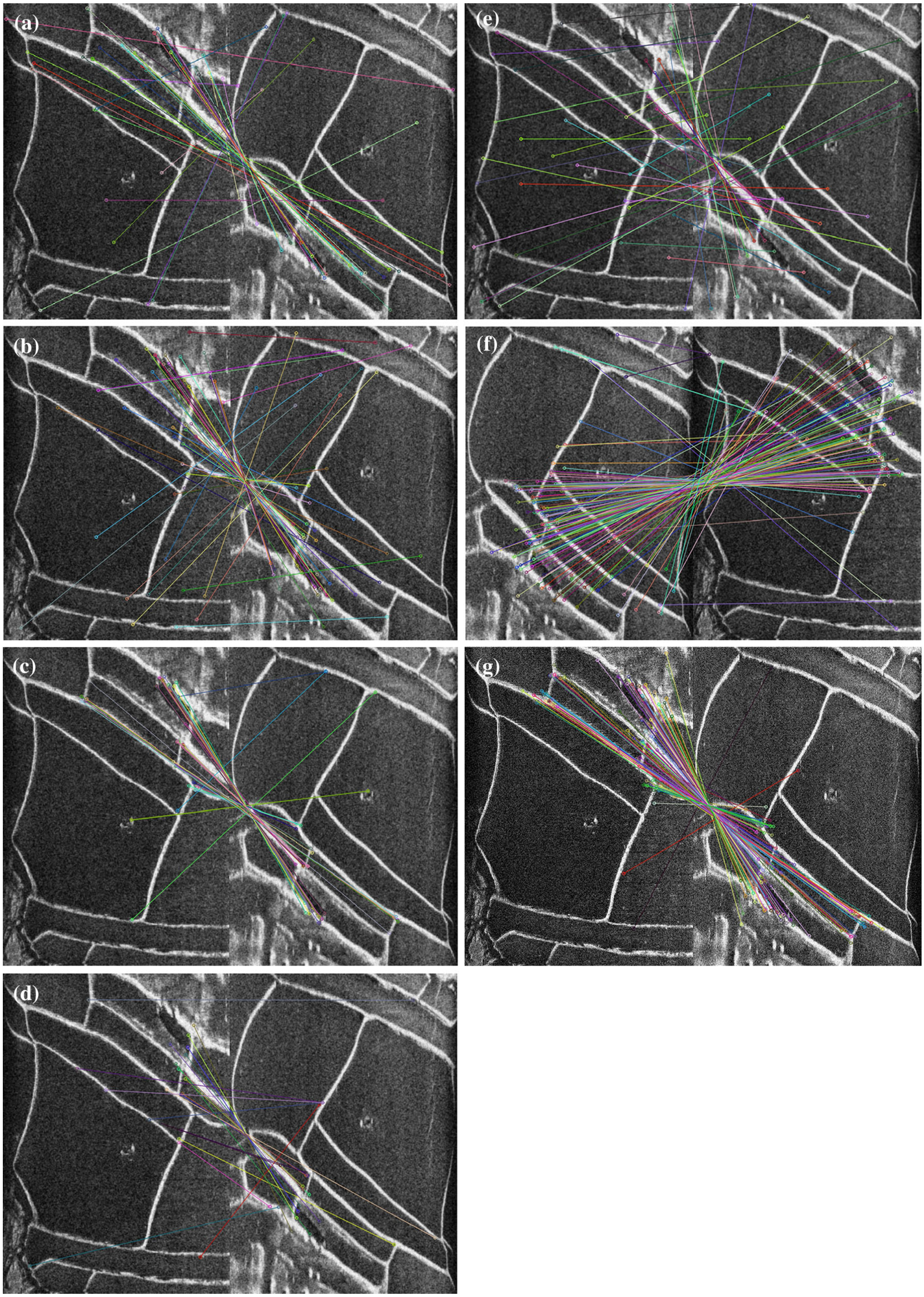

Fig. 8 Side-scan sonar image matching example with different algorithms: **a** SIFT, **b** SURF, **c** ORB, **d** FREAK, **e** bilateral SIFT, **f** KAZE, **g** proposed method

3.99 GB of RAM. The code is implemented in C++ based on OpenCV. Features are typically matched using the strategy of nearest-neighbor distance ratio (NNDR), which was developed by Lowe [6] and the strategy of random sample consensus (RANSAC), which was developed by Fischler and Bolles [22].

Figure 7 shows two side-scan images at different scales obtained by side-scan sonar from the opposite direction, which are corrupted by noise. For comparison, existing state-of-the-art algorithms are shown in Fig. 8; Fig. 8a–f shows images matched using SIFT, SURF, ORB, FREAK, BFSIFT and KAZE, and Fig. 8g shows the results of our method. Table 2 shows the effect of μ on the matching result, the P-M equation with $\mu = 2$ had the lowest match rate, the match rate reached highest when $\mu = 4$ and went down when $\mu > 4$, that was because the diffusion equation over-smoothed detailed information of the image, which was consistent with the result in Table 1. The data listed in Table 3 show that the SIFT, SURF, ORB, BFSIFT and FREAK algorithms had the lowest performance of match from the noisy data, and mismatched most keypoints with strategy of NNDR and RANSAC. So it is clear that methods based on linear scale space did not work well when applying to side-scan sonar images. KAZE gave a high match rate compared to the formal methods, however, mismatches are still obvious. The proposed method gave the highest match rates because the nonlinear diffusion filter with the modified P-M equation preserves more edge and detailed information, so that the features are preserved and can be extracted more accurately.

Table 2 Effect of value μ on the matching result

μ	2	3	4	6	9
Match rate	35.6 %	36 %	60 %	11 %	10.4 %

Table 3 Comparison of the matching algorithms

Method	Total keypoints	Correct matched keypoints	Match rate (%)
SIFT + RANSAC	981	41	4.2
SURF + RANSAC	1661	51	3.1
ORB + RANSAC	500	60	12
FREAK + RANSAC	275	23	8.4
BFSIFT + RANSAC	1014	44	4.3
KAZE + RANSAC	416	148	35.6
Proposed method	175	105	60

Table 4 Time consumption

Method	Feature detection and description time (s)
SIFT + RANSAC	3.4
SURF + RANSAC	3.6
ORB + RANSAC	0.27
FREAK + RANSAC	0.23
BFSIFT + RANSAC	5.1
KAZE + RANAC	2.36
Proposed method	2.25

Table 4 lists the computational time for the image matching; ORB and FREAK were the fastest methods because they do not build a scale space when detecting keypoints, and they use binary strings to speed up the feature description. It is interesting that SURF cost more time than SIFT, maybe because the SIFT code in OpenCV was optimized. Note that BFSIFT, which used the latest edge-preserving smoothing method, detected more keypoints and matched a little more than SIFT; however, due to the complexity of the bilateral filter for constructing scale space, the time consumed was about 1.5 times as high as SIFT. However, our method was comparable to the KAZE algorithms and performed better than any of the other matching algorithms.

We built a dataset of sonar images with different conditions to test the performance of our method. The sonar images had severe noise degradation, as shown in Fig. 9. The resolution of the datasets PLAIN, WRECK, and TERRACE were 503×700, 529×619, and 989×466 pixels, respectively. The results of the evaluation are shown in Fig. 10. Our method required more time for computation than the ORB and FREAK methods; however, ours was faster than any of the other algorithms, and the matching rate was the highest of all the methods.

5 Conclusions

We have described a feature-matching algorithm based on a nonlinear scale space constructed using a nonlinear diffusion equation for side-scan sonar image applications. We

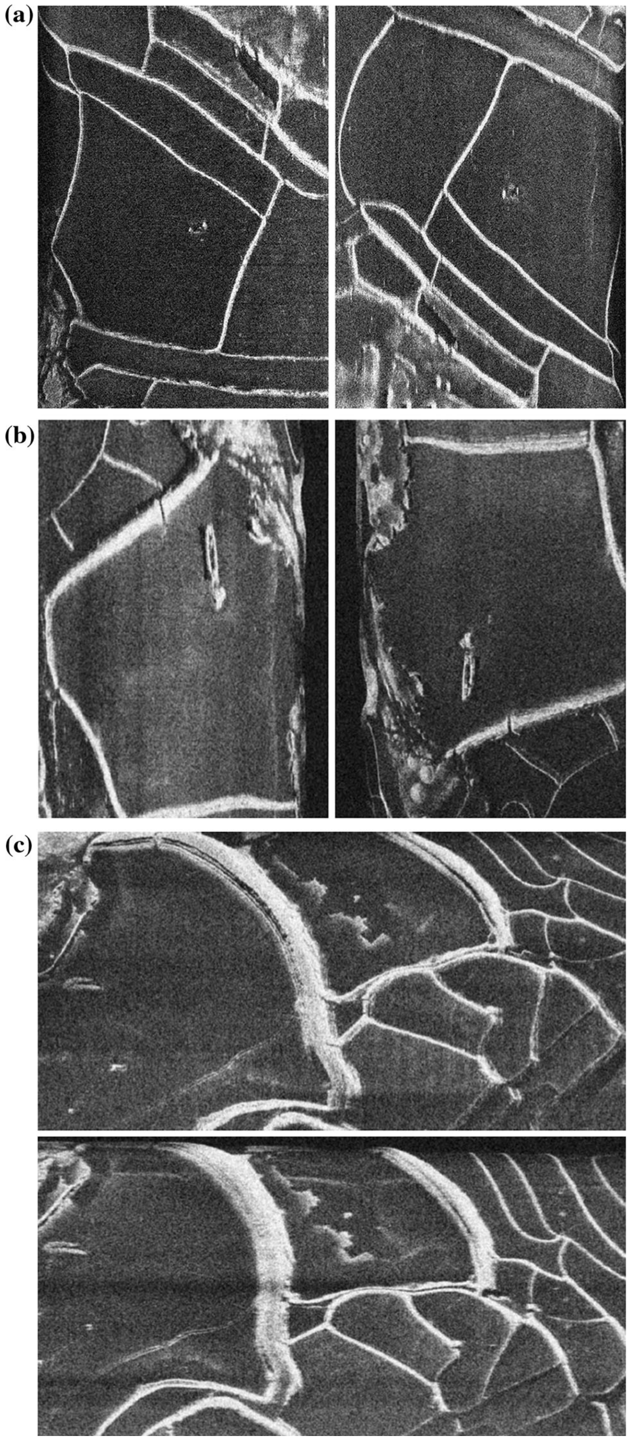

Fig. 9 Dataset of sonar images: **a** PLAIN, **b** WRECK, **c** TERRACE

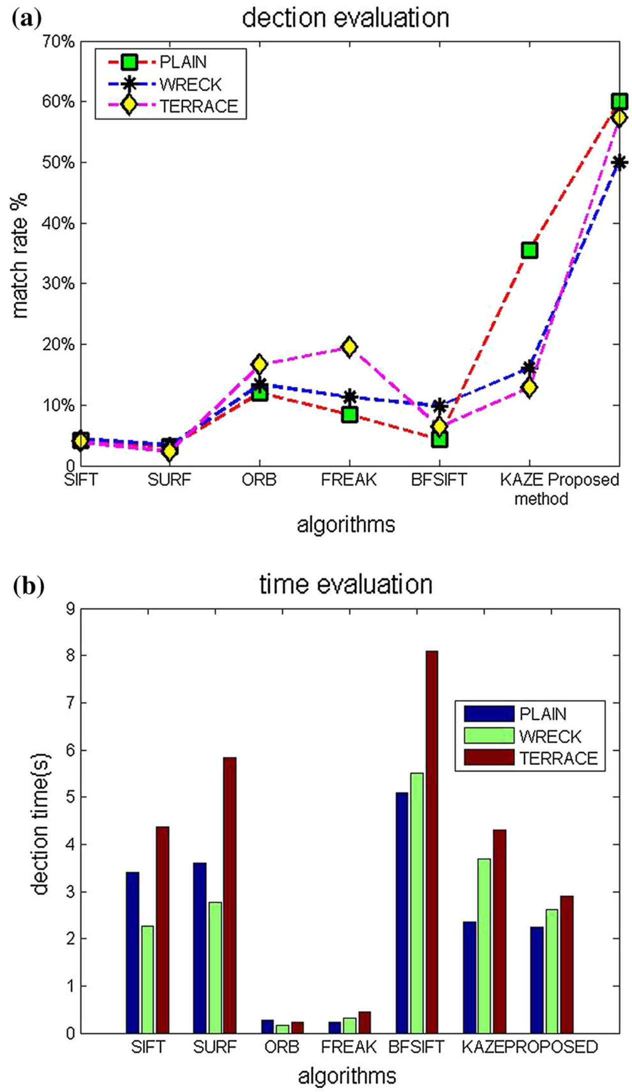

Fig. 10 Detection and time evaluation result. **a** Detection evaluation, **b** Time evaluation

achieved excellent noise-reduction performance using the nonlinear diffusion filter, and the modified P-M equation preserves much of the edge and line texture information of the sonar image. The descriptor we designed decreases the dimensionality of the feature vector. The experimental results described here demonstrate that our method outperforms the existing state-of-the-art methods.

Acknowledgments This research was supported by Natural Science Foundation of Heilongjiang Province of China (Grant No. F201416) and National Natural Science Foundation of China (Grant No. 61375094).

References

1. Ye X-F, Zhang Z-H, Liu PX, Guan H-L (2010) Sonar image segmentation based on GMRF and level-set models. Ocean Eng 37(10):891–901
2. Son-Cheoi Yu (2008) Development of real-time acoustic image recognition system using by autonomous marine vehicle. Ocean Eng 35(1):90–105

3. Daniel S, Le Ĺeannec F (1998) Side-scan sonar image matching. IEEE J Ocean Eng 23(3):245–259
4. Rominger C, Martin A, Khenchaf A, Laanaya H (2009) Sonar image registration based on conflict from the theory of belief functions. Information Fusion, 2009. FUSION '09. 12th international conference on, 1317–1324
5. Khater HA, Gad AS, Omran EA, Abdel-Fattah AA (2009) Enhancement matching algorithms using fusion of multiple similarity metrics for sonar images. World Appl Sci J 6(6):759–763
6. Vanish P, Vardy A, Walker D, Dobre OA (2011) Side-scan he for AUV navigation. 2011 IEEE symposium on and 2011 workshop on scientific use of submarine cables and related technologies (SSC), 1–7
7. Lowe DG (2004) Distinctive image features from scale-invariant keypoints. Int J Comput Vis (IJCV) 60(2):91–110
8. Yan K, Sukthankar R (2004) PCA-SIFT: a more distinctive representation for local image descriptors. In: Proceedings of the conference on computer vision and pattern recognition (CVPR), Washington, USA. IEEE 1, 511–517
9. Bay H, Tuytelaars T, Van Gool L (2006) SURF: speeded up robust features. In: Proceedings of the European conference on computer vision, vol 3951, pp 404–417
10. Lee D, Kim G, Kim D, Choi H-t (2012) Vision-based object detection and tracking for autonomous navigation of underwater robots. Ocean Eng 48:59–68
11. Abdel-Hakim AE, Farag AA (2006) CSIFT: a SIFT descriptor with color invariant characteristics. In: Proceedings of the 2006 IEEE computer society conference on computer vision and pattern recognition (CVPR'06), 2:1978–1983
12. Mikolajczyk K, Schmid C (2005) A performance evaluation of local descriptors. IEEE Trans Pattern Anal Mach Intell (PAMI) 27(10):1615–1630
13. Morel JM, Yu G (2009) ASIFT: a new framework for fully affine invariant image comparison. SIAM J Imaging Sci 2(2):438–469
14. Rublee E, Rabaud V, Konolige K, Bradski G (2011) ORB: an efficient alternative to SIFT or SURF. In: Proceedings of IEEE international conference on computer vision (ICCV), pp 2564–2571
15. Alahi A, Ortiz R, Vandergheynst P (2012) FREAK: fast retina keypoint. In: IEEE conference on computer vision and pattern recognition (CVPR), Rhode Island, Providence, USA, pp 510–517
16. Alcantarilla PF, Bartoli A, Davison AJ (2012) KAZE features. In: European conference on computer vision (ECCV), pp 2–9
17. Wang S, You H, Fu K (2012) BFSIFT: a novel method to find feature matches for SAR image registration. Geosci Remote Sens Lett IEEE 9(4):649–653
18. Perona P, Malik J (1990) Scale-space and edge detection using anisotropic diffusion. IEEE Trans Pattern Anal Mach Intell (PAMI) 12(7):629–639
19. Catte F, Lions PL, Morel JM, Coll T (1992) Image selective smoothing and edge detection by nonlinear diffusion. SIAM J Numer Anal. 29(1):182–193
20. Martinez-Baena J, Fdez-Valdivia J, Garcia JA (1997) A multichannel auto-focusing scheme for gray-level shape scale detection. Pattern Recognit (PR) 30(10):1769–1786
21. Weickert J, ter Romeny BH, Viergever M (1998) A Efficient and reliable schemes for nonlinear diffusion filtering. IEEE Trans Image Process (IP) 7:398–410
22. Fischler MA, Bolles RC (1981) Random sample consensus: a paradigm for model fitting with applications to image analysis and automated cartography. Commun ACM 24(6):381–395